Journal of Crystal Growth 484 (2018) 78–85

Contents lists available at ScienceDirect

Journal of Crystal Growth

journal homepage: www.elsevier.com/locate/crys

Numerical study of melt flow under the influence of heater-generating magnetic field during directional solidification of silicon ingots

Zaoyang Li [a,b,*], Xiaofang Qi [a], Lijun Liu [a], Genshu Zhou [b]

[a] School of Energy and Power Engineering, Xi'an Jiaotong University, Xi'an, Shaanxi 710049, China
[b] State Key Laboratory for Mechanical Behavior of Materials, Xi'an Jiaotong University, Xi'an, Shaanxi 710049, China

ARTICLE INFO

Article history:
Received 1 October 2017
Received in revised form 18 December 2017
Accepted 21 December 2017
Available online 27 December 2017
Communicated by J.J. Derby

Keywords:
A1. Computer simulation
A1. Fluid flows
A1. Magnetic fields
A1. Directional solidification
B2. Silicon

ABSTRACT

The alternating current (AC) in the resistance heater for generating heating power can induce a magnetic field in the silicon melt during directional solidification (DS) of silicon ingots. We numerically study the influence of such a heater-generating magnetic field on the silicon melt flow and temperature distribution in an industrial DS process. 3D simulations are carried out to calculate the Lorentz force distribution as well as the melt flow and heat transfer in the entire DS furnace. The pattern and intensity of silicon melt flow as well as the temperature distribution are compared for cases with and without Lorentz force. The results show that the Lorentz force induced by the heater-generating magnetic field is mainly distributed near the top and side surfaces of the silicon melt. The melt flow and temperature distribution, especially those in the upper part of the silicon region, can be influenced significantly by the magnetic field.

© 2017 Elsevier B.V. All rights reserved.

1. Introduction

The photovoltaics (PV) industry is growing fast, which is evidenced by the data that the compound annual growth rate of PV installation was 42% during the past 15 years [1] and the cumulative PV capacity installed worldwide exceeded 300 GWp by 2016 [2]. Silicon ingot manufactured by directional solidification (DS) method is the main material for solar cells and the market share is more than 60% [2]. Therefore, it's essential to study the DS process and improve the silicon ingot quality for promoting the development of PV industry. The DS is a highly coupled nonlinear thermal process with complex interactions among the silicon melt flow, argon flow and different solid components [3]. In particular, the silicon melt flow can influence the temperature distribution, impurities transport and crystallization interface shape significantly [4,5]. Therefore, a deep and comprehensive understanding of the melt flow characteristics is crucial for optimization and control of the DS process.

Some researchers carried out global or local simulations of heat transfer and fluid flow in the DS furnace to study the influence of growth parameters on silicon melt flow [5–8]. The thermal buoyancy force is considered as the main driving force for the melt flow in these studies. In order to actively control the melt flow, some researchers designed various magnetic fields and studied the influence of Lorentz forces on flow pattern and intensity. For example, Vizman et al. [9,10] numerically studied the 3D silicon melt flow in the DS of silicon ingots with different types of magnetic fields, including vertical magnetic field (VMF), horizontal magnetic field (HMF) and traveling magnetic field (TMF). Li et al. [11] experimentally studied the effect of alternating magnetic field (AMF) on the melt flow, which can influence the removal of metal impurities in silicon ingots. In order to apply the magnetic field conveniently, Rudolph et al. [12,13] developed a heater-magnet module that can generate heating power and a TMF in the crystal growth furnace simultaneously. Dropka et al. [14] studied the influence of such a TMF on silicon melt flow and crystallization interface shape in a DS furnace. The above studies show that the Lorentz force induced by an appropriate magnetic field can suppress the thermal buoyancy force, control the silicon melt flow and influence the DS process.

In the general industrial DS furnace with resistance heating [5,15], an external magnetic field is rarely applied to control the silicon melt flow due to high cost and complex design. However, the alternating current (AC) in the heater for generating heating power can induce an internal magnetic field. This kind of heater-generating magnetic field exists in the general industrial DS process and is not specially designed, which is different from the above-mentioned TMF generated by the specially designed

* Corresponding author at: School of Energy and Power Engineering, Xi'an Jiaotong University, Xi'an, Shaanxi 710049, China.
E-mail address: lizaoyang@mail.xjtu.edu.cn (Z. Li).

https://doi.org/10.1016/j.jcrysgro.2017.12.033
0022-0248/© 2017 Elsevier B.V. All rights reserved.

heater-magnet module [12–14]. The heater-generating magnetic field may influence the melt flow and crystal growth significantly, whereas little research has been devoted to this topic. Therefore, we carry out 3D global numerical simulations in this paper to study the distribution of Lorentz force induced by the heater-generating magnetic field as well as its influence on silicon melt flow, temperature distribution and other crystal growth parameters in an industrial DS furnace.

2. Model description

The configuration and dimensions of the DS furnace for casting silicon ingots have been introduced in a previous study [15]. The furnace includes silicon region, quartz crucible, graphite susceptors, graphite heater, carbon felt insulations and other components. The physical properties of all these component materials can be found in Table 1 and Ref. [15]. Fig. 1 shows the schematic diagrams of the core parts in the DS furnace including silicon melt and graphite heater. The volume of the cuboid silicon melt region is $0.84 \times 0.84 \times 0.26\ m^3$, and therefore the finally solidified silicon ingot is about 450 kg. A snakelike graphite heater is around the silicon region and three electrodes labeled with A, B and C are connected to it. A three-phase AC is connected to the three electrodes to generate heating power in the graphite heater. It's obvious that the three-phase AC is in delta connection, as shown in Fig. 1(c). The expressions of the three-phase AC in this study are:

$$I_A = 1742 \sin(100\pi t), \tag{1}$$

$$I_B = 1742 \sin(100\pi t + 2\pi/3), \tag{2}$$

$$I_C = 1742 \sin(100\pi t + 4\pi/3). \tag{3}$$

The above equations indicate that the current amplitude is 1742 A, the angular frequency is 100π, the frequency is 50 Hz and the phase difference is 120°. The three-phase AC can generate a total heating power of 56 kW to guarantee that the temperature at the silicon bottom is higher than the melting point of 1685 K and the silicon feedstock is fully melted. At the same time, a non-steady magnetic field arises due to the phase shift between the three delta-connected heater segments, as shown in Fig. 1(c). The heater-generating magnetic field can induce Lorentz force in the silicon melt and may influence the flow pattern and intensity.

As the frequency of the magnetic field is much higher than that of the silicon melt flow, the periodic Lorentz force can be averaged over one time period. The software ANSYS Maxwell is applied to calculate the distributions of magnetic field and Lorentz force in the silicon melt. To guarantee that the software is used correctly and the numerical method is appropriate, the generation of a TMF is first solved according to a previous study [16]. The results show that the Lorentz force calculated by Maxwell is in good agreement with that in this reference. For the accurate calculation of 3D magnetic field in this study, the adaptive mesh refinement and skin depth meshing techniques are applied, and the number of the final mesh is about 920,000.

Table 1
Physical properties for silicon melt and graphite heater.

Material	Variable	Value
Silicon	Density (kg/m^3)	2530
	Specific heat (J/kg·K)	900
	Thermal conductivity (W/m·K)	64
	Dynamic viscosity (kg/m·s)	7×10^{-4}
	Thermal expansion coefficient (1/K)	1.36×10^{-4}
	Melting point (K)	1685
	Emissivity	0.3
	Electrical conductivity (S/m)	1×10^6
	Relative magnetic permeability	1
Graphite	Density (kg/m^3)	1830
	Specific heat (J/kg·K)	1800
	Thermal conductivity (W/m·K)	100
	Emissivity	0.8
	Electrical conductivity (S/m)	1×10^5

To study the influence of magnetic field on silicon melt flow, the 3D global simulations of fluid flow and heat transfer in the entire DS furnace are carried out. The simulations include silicon melt flow, argon gas flow, solid thermal conduction and thermal radiation. In silicon melt, the Boussinesq approximation is applied to describe the thermal buoyancy force due to density change. Therefore, the governing equations for melt flow are:

$$\nabla \cdot \vec{u} = 0, \tag{4}$$

$$\rho \frac{\partial \vec{u}}{\partial t} + \rho \vec{u} \cdot \nabla \vec{u} = -\nabla p + \nabla \cdot [\mu(\nabla \vec{u} + \nabla \vec{u}^T)] - \rho \vec{g} \beta_T (T - T_{ref}) + \vec{F}_L, \tag{5}$$

$$\rho C_p \frac{\partial T}{\partial t} + \rho C_p \vec{u} \cdot \nabla T = \lambda \nabla \cdot (\nabla T), \tag{6}$$

where $\vec{u}$ is the velocity, ρ is the density, t is the time, p is the pressure, μ is the dynamic viscosity, $\vec{g}$ is the gravity acceleration vector, β_T is the thermal expansion coefficient, T is the temperature, T_{ref} is the reference temperature and C_p is the specific heat capacity. $\vec{F}_L$ is the time-averaged density of Lorentz force induced by the heater-generating magnetic field.

For the boundary condition settings, the temperature continuity and heat flux conservation are kept at all interior boundaries between any two different computational domains. No-slip condition is applied at all solid walls in the argon gas and silicon melt domains. Along the melt free surface, both the normal velocity component and the shear stress are set to zero. In the DS process for silicon ingots, the isotherms in the silicon melt are usually flat and the radial temperature gradient along the melt free surface is small [10]. This means the Marangoni force is very weak and its influence on melt flow is limited to the region near the free surface [10]. Therefore, the Marangoni force is not important in the case discussed in this paper and it's neglected in this study to make clear analyses of the effects of Lorentz force. The temperature of the furnace outer wall is assumed to 300 K, and the inlet temperature and pressure of argon gas are set to 300 K and 60,000 Pa, respectively. A total mesh number of 2,300,000 is applied for the entire DS furnace, and the mesh number for silicon melt region is 384,000. The above 3D numerical model for fluid flow and heat transfer in the DS furnace is established by using the software ANSYS Fluent, and it has been validated by comparing the numerical results with the experimental data [17].

3. Results and discussion

3.1. Lorentz force density

To study the influence of heater-generating magnetic field on silicon melt flow and other crystal growth parameters, the distributions of Lorentz force density are first calculated. Fig. 2 shows several isosurfaces of the magnitude of Lorentz force density $|\vec{F}_L|$ in silicon melt. The expression of $|\vec{F}_L|$ is:

$$|\vec{F}_L| = \sqrt{\vec{F}_X^2 + \vec{F}_Y^2 + \vec{F}_Z^2}, \tag{7}$$

where $\vec{F}_X$, $\vec{F}_Y$ and $\vec{F}_Z$ are the vector components of Lorentz force density in X, Y and Z directions, respectively. The maximum value

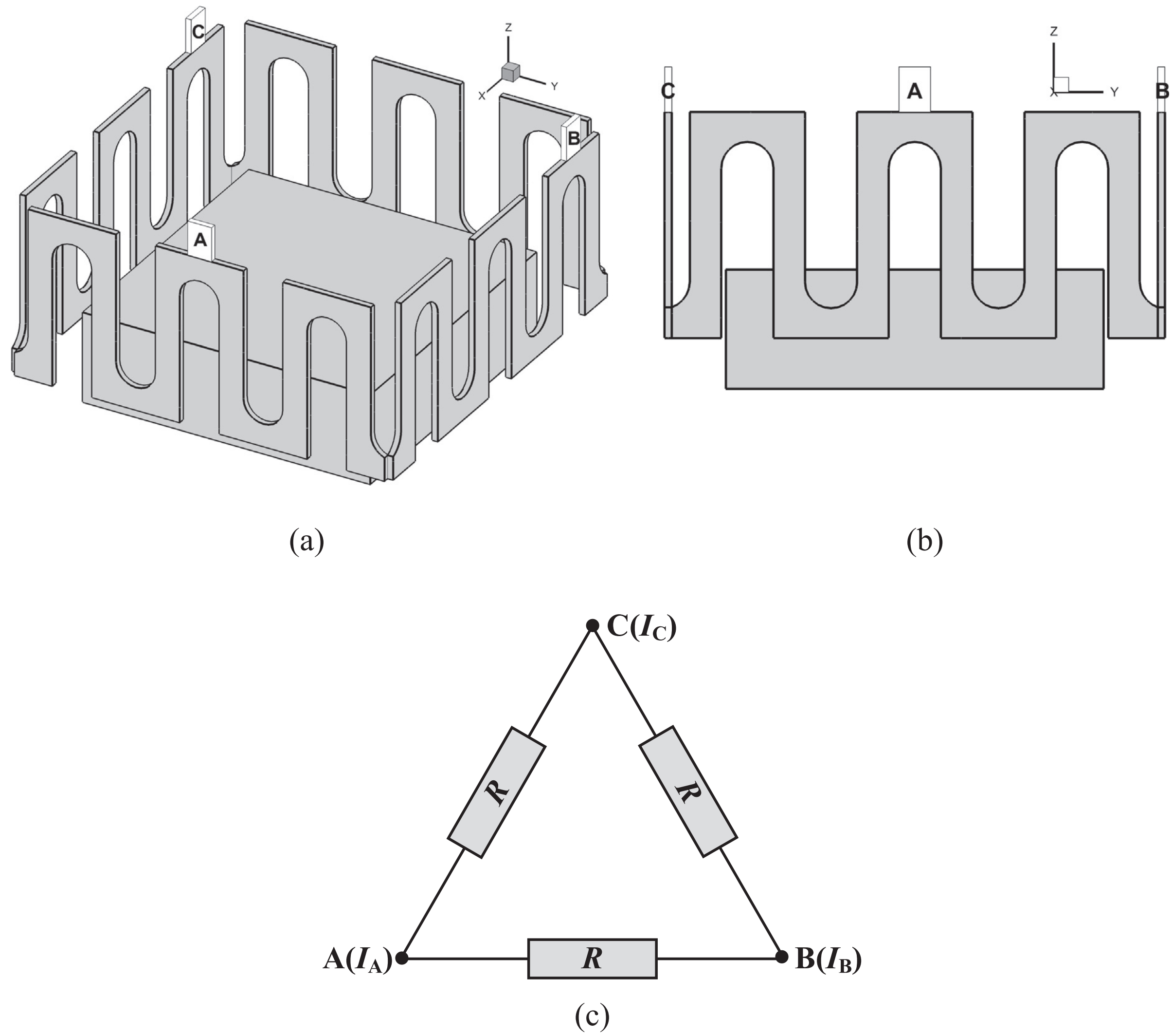

Fig. 1. Schematic of silicon melt region and graphite heater in the DS furnace: (a) 3D top view; (b) front view; (c) delta connection of the three-phase AC.

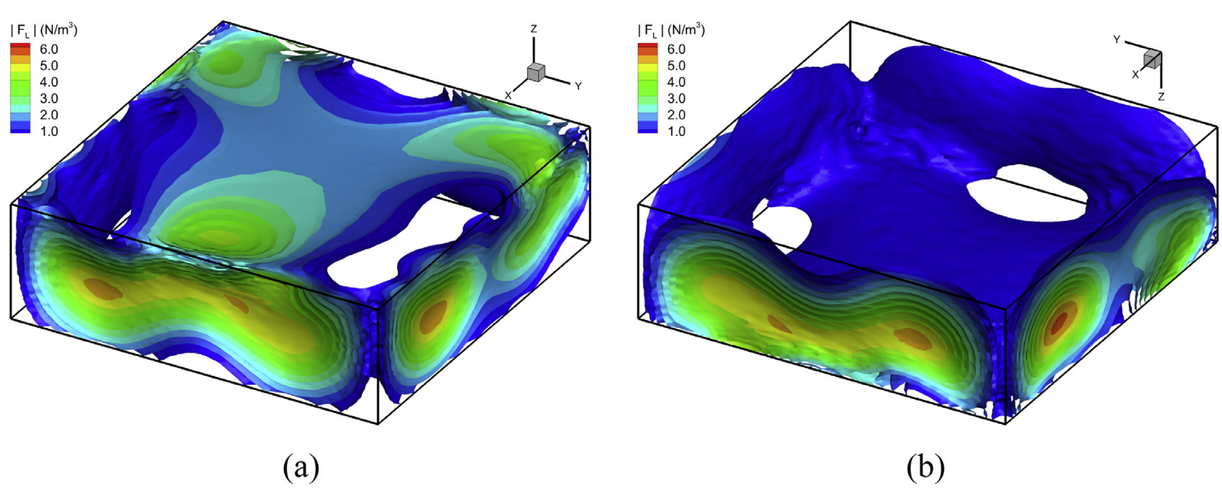

Fig. 2. Isosurfaces of the magnitude of Lorentz force density in silicon melt: (a) 3D top view; (b) 3D bottom view.

of $|\vec{F}_L|$ is about 6.0 N/m^3 and the range shown in Fig. 2 varies from 1.0 to 6.0 N/m^3. The difference between adjacent isosurfaces is 0.5 N/m^3, and therefore 11 isosurfaces are plotted in Fig. 2. It can be seen that the force is present only in the skin layer with a depth smaller than 7.1 cm, which can be estimated by the following equation:

$$\delta = \frac{1}{\sqrt{\pi \mu_0 \mu_r \sigma f}}, \tag{8}$$

where δ is the skin depth, μ_0 is the vacuum magnetic permeability, μ_r is the relative magnetic permeability of silicon melt, σ is the electrical conductivity of silicon melt and f is the frequency of AC. In Fig. 2(a), the 3D top view indicates that the maximum magnitudes of Lorentz force density at the melt top surface are located near the three electrodes. There are also high magnitude regions near the side surfaces of the silicon melt. The 3D bottom view in Fig. 2(b) shows that the magnitudes of Lorentz force density in the melt bottom and central regions are smaller than 1 N/m^3. It's because these regions are far away from the heater, as shown in Fig. 1(b). The above analyses indicate that the large Lorentz force induced by the heater-generating magnetic field is mainly distributed near the top and side surfaces of the silicon melt.

To reveal the distributions of Lorentz force direction, Fig. 3 shows the streamlines of Lorentz force density in the silicon melt. The streamlines are plotted based on the three vector components of the Lorentz force density. Only some special positions are chosen to plot the streamlines so as to clearly present the details. In Fig. 3(a1), the streamlines originating from the melt side surfaces point inwards and downwards to the melt center, and at the same time rotate in clockwise direction around the Z axis, as shown in Fig. 3(a2). In Fig. 3(b1) and (b2), the 3D top view and top view show that the streamlines originating from the melt top surface also point downwards to the melt center and turn left in the clockwise direction. The rotation direction of Lorentz force is determined by the phase order of the three-phase AC, as shown in Eqs. (1)–(3).

3.2. Melt flow and temperature distribution

The maximum magnitude of Lorentz force density is about 6 N/m^3, which is large enough to influence the silicon melt flow and temperature distribution during DS of silicon ingots [16]. Therefore, the 3D views of the streamlines and temperature distribution in the silicon melt with and without Lorentz force are first compared to make a preliminary analysis of the effect of the heater-

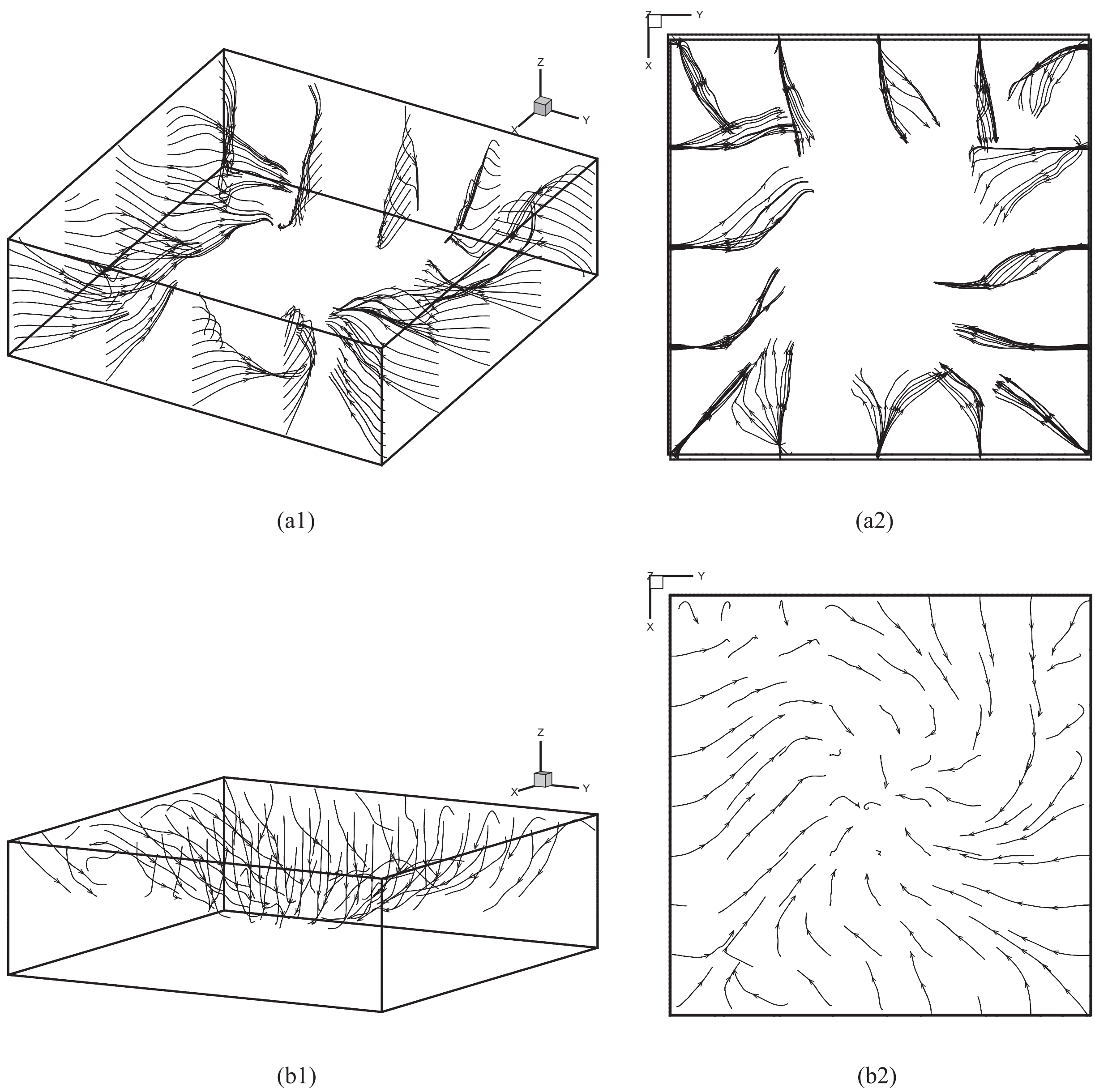

Fig. 3. Streamlines of Lorentz force density in the silicon melt: (a1, 3D top view; a2, top view) originating from melt side surfaces; (b1, 3D top view; b2, top view) originating from melt top surface.

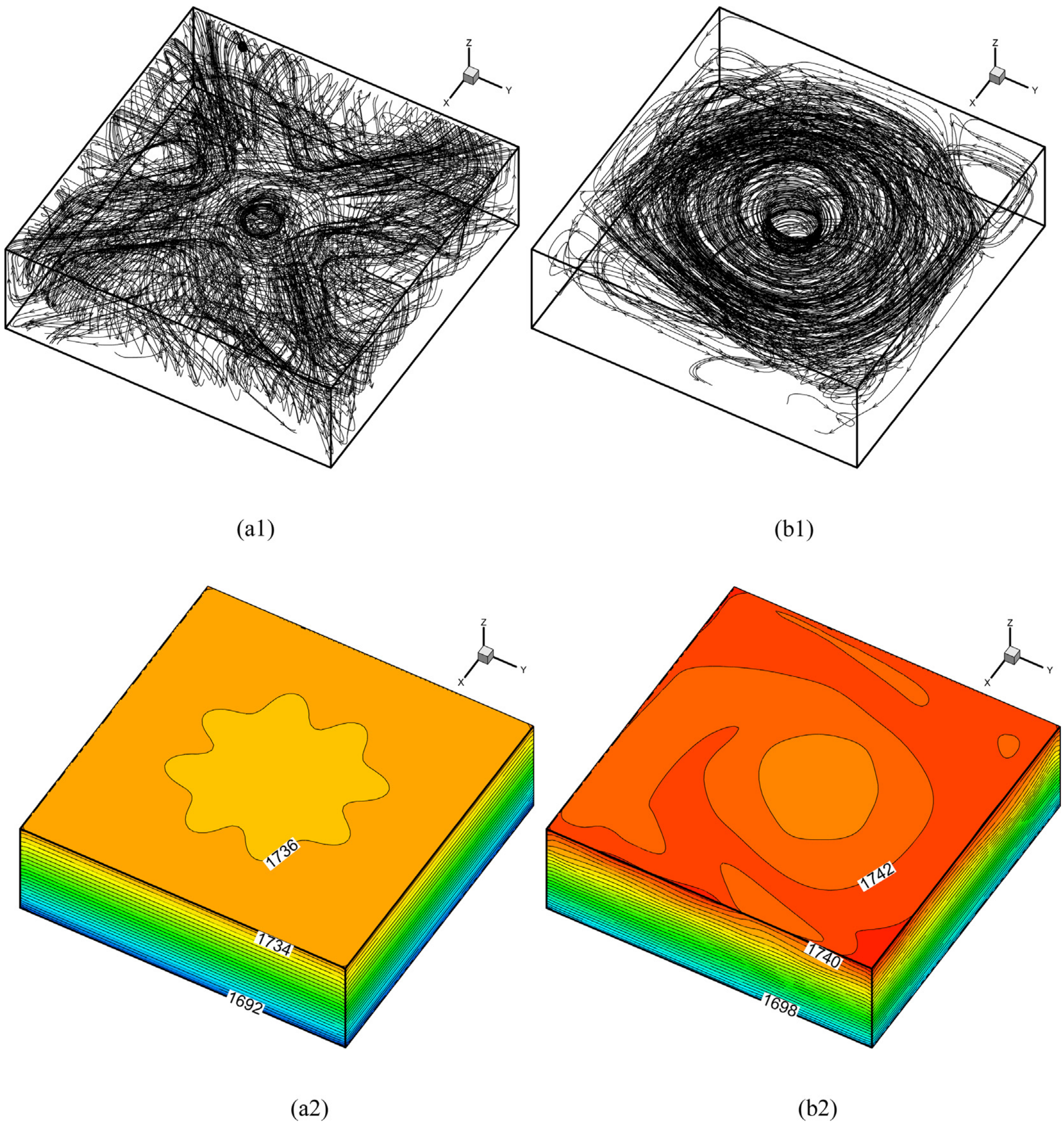

Fig. 4. Distributions of streamlines (a1 and b1) and temperature (a2 and b2, 2 K between isotherms) in silicon melt under different conditions: (a1, a2) only thermal buoyancy is considered; (b1, b2) both thermal buoyancy force and Lorentz force are considered.

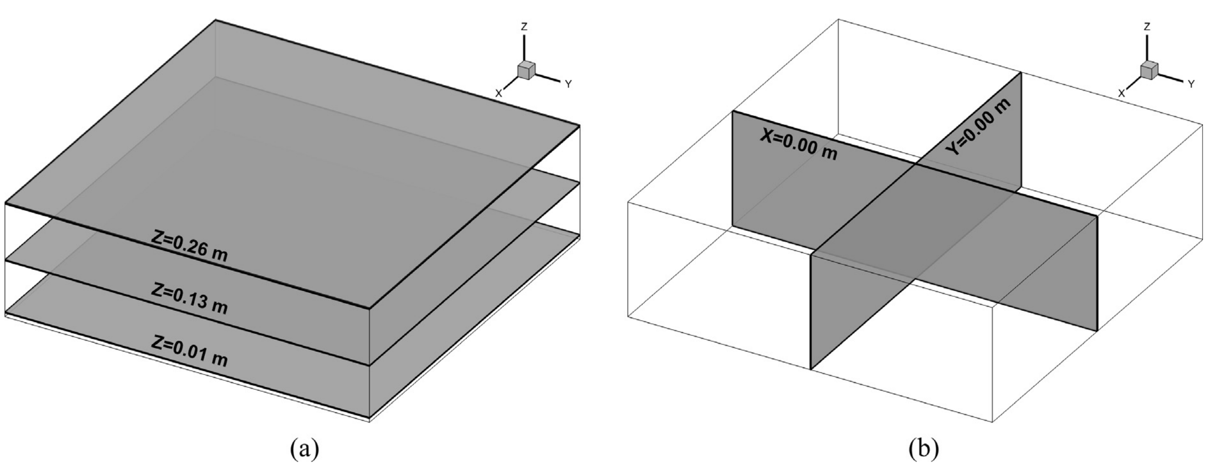

Fig. 5. Positions of different sections: (a) X-Y sections; (b) Y-Z and X-Z sections.

generating magnetic field, as shown in Fig. 4. The streamlines present a cross shape in the diagonal direction accompanied by a small circle in the melt center in Fig. 4(a1) when only the thermal buoyancy force drives the silicon melt flow. This kind of flow pattern is centrosymmetric and also leads to a centrosymmetric temperature distribution, as shown in Fig. 4(a2). Once the effect of

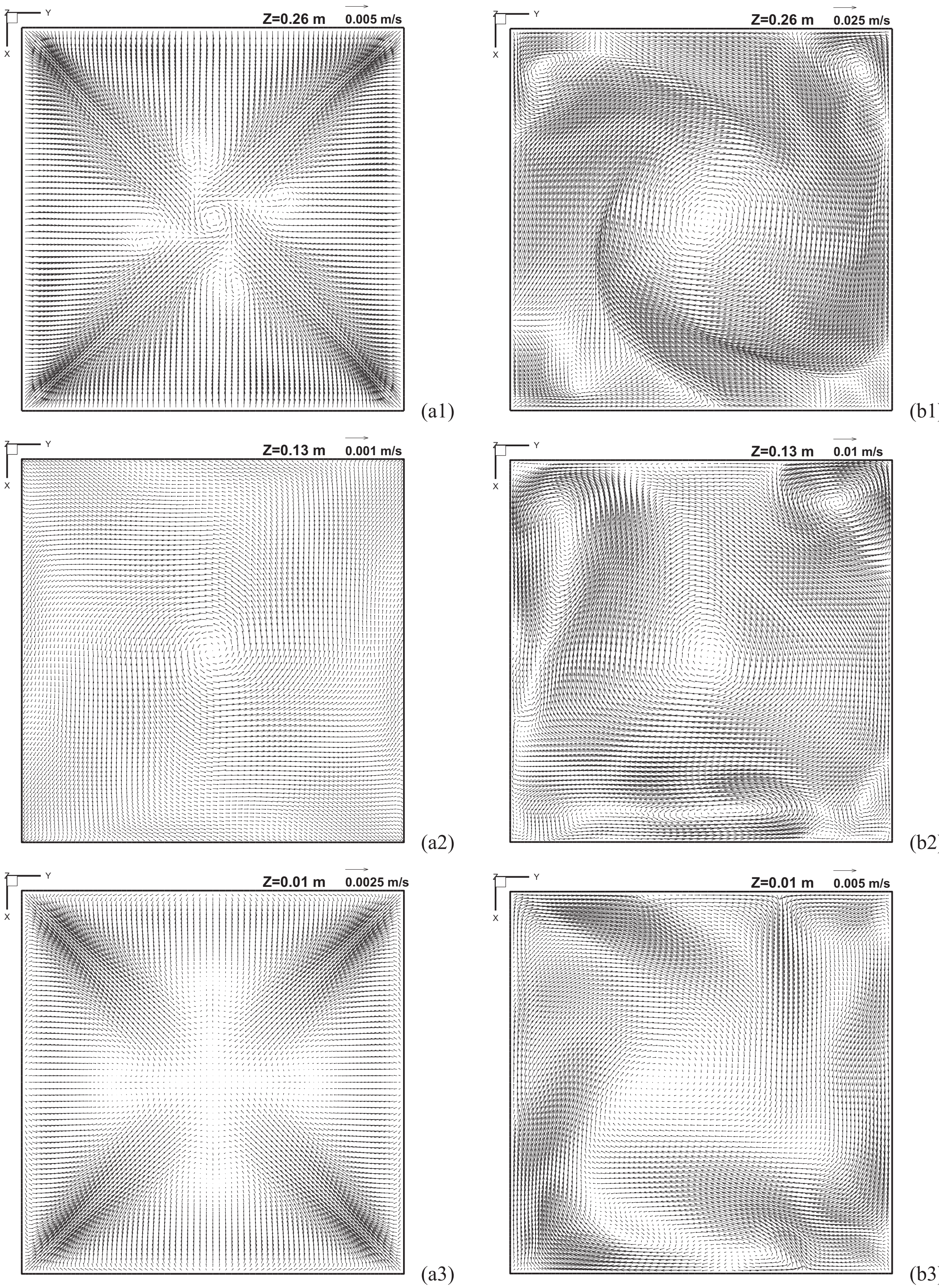

Fig. 6. Velocity vectors of silicon melt in X-Y sections under different conditions: (a1–a3) only thermal buoyancy is considered; (b1–b3) both thermal buoyancy force and Lorentz force are considered.

Lorentz force is considered, the silicon melt begins to rotate in the clockwise direction, and the streamlines and temperature distribution become non-centrosymmetric, as shown in Fig. 4(b1) and (b2). The clockwise melt flow is induced by the Lorentz force in the same direction, and therefore the flow direction will be counter-clockwise if the AC phase order is opposite. Due to the change of melt flow, the temperature in the silicon region rises significantly in Fig. 4(b2) compared with the case in Fig. 4(a2).

To study the influence of heater-generating magnetic field on silicon melt flow in detail, the melt velocity vectors in different horizontal and vertical sections are analyzed. Fig. 5 shows the positions of these sections, for which the origin of the Cartesian coordinate system is located at the bottom center of the silicon melt.

Fig. 6 shows the melt velocity vectors consisting of X and Y components in the horizontal sections. The velocity vectors present centrosymmetric characteristics in Fig. 6(a1–a3) when thermal buoyancy force is the only driving force for melt flow. In the top and bottom sections, as shown in Fig. 6(a1) and (a3), the silicon melt flows from side boundaries to central parts. Several small vortices are induced in the top section when the inward flows encounter. The scales of velocity vectors indicate that the melt flow is strong in the top and bottom sections, whereas it's extremely weak in the middle section. The above melt flow characteristics are closely related to the temperature distribution in the silicon melt, which will be analyzed in Fig. 7.

Both the thermal buoyancy force and the Lorentz force induced by the heater-generating magnetic field are considered in Fig. 6(b1–b3). The velocity vectors of silicon melt are non-centrosymmetric and rotate in the clockwise direction in all three sections, which means the Lorentz force is dominant for the melt flow. By comparing the scales of velocity vectors, it can be found that the melt flow becomes weaker and weaker from top to bottom sections, which is different from the cases without Lorentz force. This is because the Lorentz force decreases significantly from melt top to bottom, as shown in Fig. 2.

The distributions of velocity vectors and temperature in vertical sections for cases with and without Lorentz force are shown in Fig. 7. The melt flow and temperature distribution are centrosymmetric under the influence of thermal buoyancy force, and therefore only the central Y-Z section is chosen for analysis, as shown in Fig. 7(a1) and (a2). In Fig. 7(a1), there are two couples of strong vortices in the top and bottom regions with a weak flow in the middle region. The melt flow is axisymmetric, and the top and bottom vortices flow upwards and downwards along the side boundaries, respectively. It's obvious that the flow patterns are induced by the temperature distribution in the silicon melt, as shown in Fig. 7(a2).

As the melt flow and temperature distribution are non-centrosymmetric under the influence of Lorentz force, both the central Y-Z and X-Z sections are chosen for analysis, as shown in Fig. 7(b1), (b2), (c1) and (c2). The melt flow in the silicon upper region is non-axisymmetric and stronger in Fig. 7(b1) and (c1) compared with the case in Fig. 7(a1). Therefore, the isotherms are not flat in this region and the mixing of melt is enhanced. In the melt central region, the mixing is slightly stronger and the vertical temperature difference between the maximum and minimum values decreases from 40 K in Fig. 7(a2) to 38 K in Fig. 7(b2) and (c2). In the melt side region, the mixing is relatively weak due to the influence of solid crucible wall, and therefore the vertical temperature difference is almost the same for the three cases. The strong melt flow induced by the Lorentz force also enhances the vertical heat transfer through the silicon melt, which means more heat is released from the melt bottom to its surroundings. The surroundings temperature is almost fixed, and therefore the tempera-

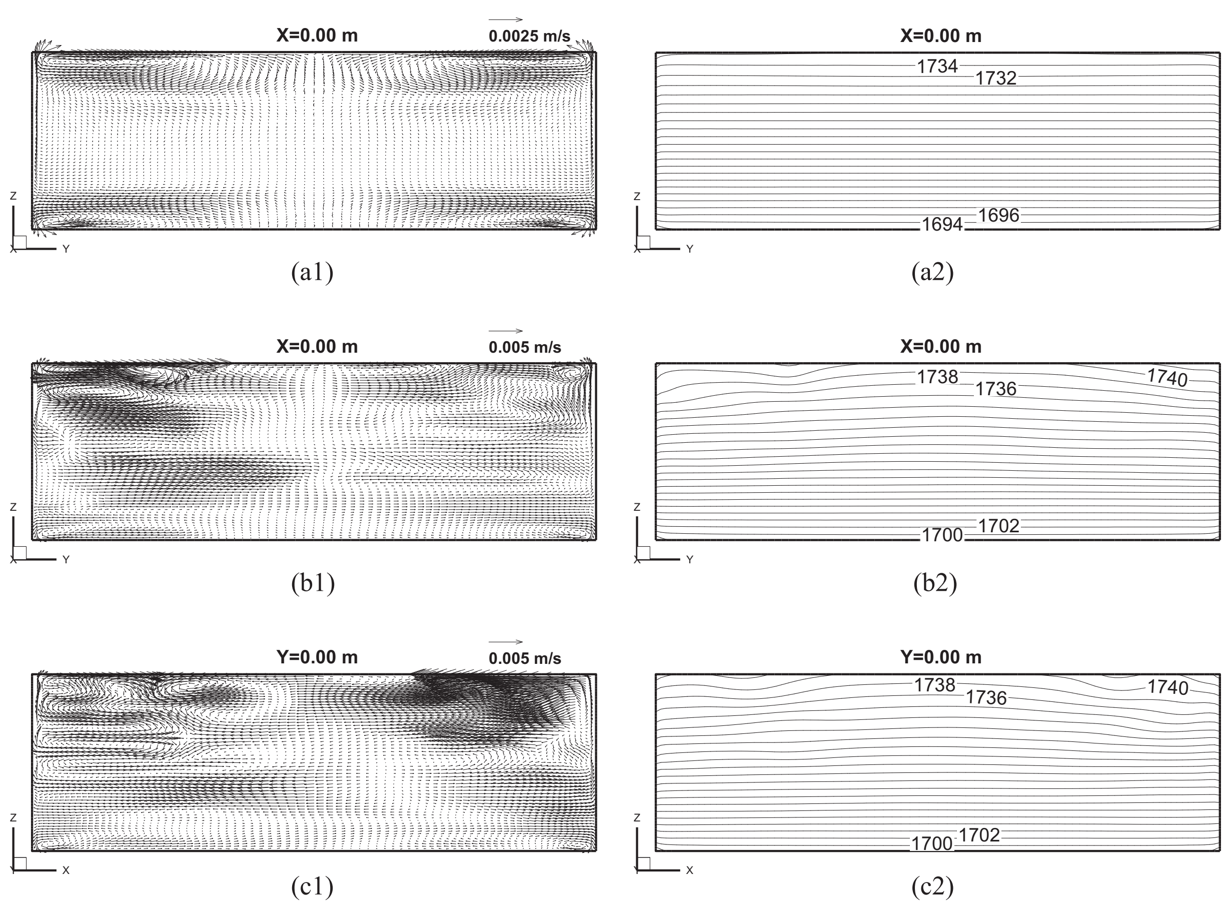

Fig. 7. Distributions of velocity vectors (a1, b1 and c1) and temperature (a2, b2 and c2, 2 K between isotherms) under different conditions: (a1, a2) Y-Z section, only thermal buoyancy is considered; (b1, b2) Y-Z section, both thermal buoyancy force and Lorentz force are considered; (c1, c2) X-Z section, both thermal buoyancy force and Lorentz force are considered.

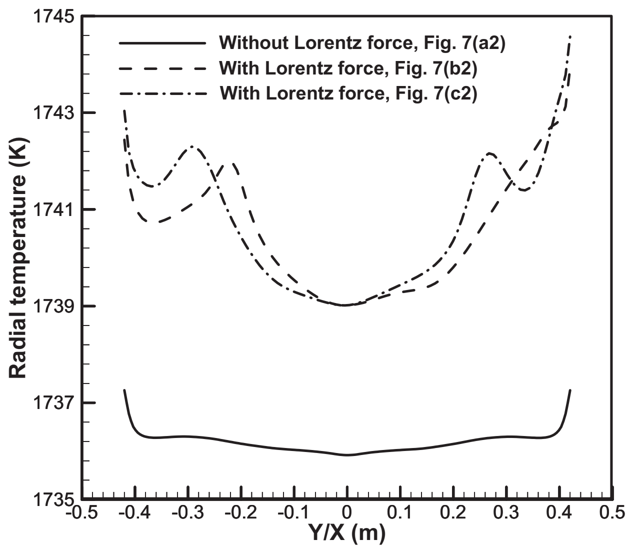

Fig. 8. Radial distributions of temperature on silicon melt top surface.

ture at melt bottom and that in the whole silicon melt rises about 4–6 K.

To quantitatively analyze the effects of melt flow on isotherm shape, Fig. 8 shows the typical radial temperature profiles along the melt top surface in Fig. 7(a2), (b2) and (c2). It's obvious that the solid line representing the case without Lorentz force is relatively flat, and the difference between the highest and lowest temperature is about 1 K. For the cases with Lorentz force, the temperature profiles are not flat anymore and the temperature difference is about 6 K.

One issue that needs further discussion is the influence of heater-generating magnetic field on the silicon crystal growth. In a general DS furnace, the heater position is usually higher than that of the silicon melt, as shown in Fig. 1, to provide downward heat flux in the silicon region and guarantee the DS of silicon ingots. Therefore, the Lorentz force generated by the magnetic field is mainly distributed near the top and side surfaces of the silicon melt, as shown in Fig. 2. The melt flow is enhanced and the flow pattern is changed significantly by the Lorentz force, as shown in Figs. 6 and 7. It is obvious that the rate and pattern of silicon melt flow is large different between the cases with and without Lorentz force. However, the strong melt flow induced by the Lorentz force is mainly distributed in the melt upper region, as shown in Figs. 6 (b1), 7(b1) and (c1). As a result, the isotherms in the melt upper region are significantly affected and become curved when the Lorentz force is considered, as shown in Fig. 7(b2) and (b3). The isotherm shapes in the melt lower region are similar and keep flat for different cases. The crystallization interface is usually considered to be consistent with the isotherm of the melting point, and therefore the interface shape at the late stage of solidification can be affected significantly. Besides the crystallization interface, the change of melt flow can also influence the impurities transport in the silicon melt and finally determines the impurities concentration in the silicon ingots.

4. Conclusions

We numerically studied the distribution of Lorentz force induced by the heater-generating magnetic field and its influence on the silicon melt flow and temperature distribution in an industrial DS furnace for silicon ingots. The results show that the Lorentz force distributed near the top and side surfaces of the silicon melt is large enough to suppress the thermal buoyancy force and influence the melt flow. Under the influence of Lorentz force, the silicon melt flow is enhanced and rotates in the horizontal plane. At the same time, the streamlines and temperature distribution become non-centrosymmetric. Due to the strong and non-centrosymmetric melt flow, the temperature in the silicon melt rises significantly and the isotherms in the melt upper region are not flat anymore. The change of melt flow and temperature distribution caused by the heater-generating magnetic field can influence the crystal growth process.

Acknowledgments

This research was supported by the National Natural Science Foundation of China (51406156), and Natural Science Basic Research Plan in Shaanxi Province of China (2016JQ5005).

References

[1] Fraunhofer Institute for Solar Energy Systems. Photovoltaics Report, Freiburg, Germany, 2016.
[2] VDMA Photovoltaic Equipment. International Technology Roadmap for Photovoltaic (eighth ed.), 2017.
[3] Z. Li, L. Liu, W. Ma, K. Kakimoto, Effects of argon flow on heat transfer in a directional solidification process for silicon solar cells, J. Cryst. Growth 318 (2011) 298–303.
[4] Z. Li, L. Liu, W. Ma, K. Kakimoto, Effects of argon flow on impurities transport in a directional solidification furnace for silicon solar cells, J. Cryst. Growth 318 (2011) 304–312.
[5] Z. Li, L. Liu, X. Liu, Y. Zhang, J. Xiong, Effects of argon flow on melt convection and interface shape in a directional solidification process for an industrial-size solar silicon ingot, J. Cryst. Growth 360 (2012) 87–91.
[6] A.T. Kuliev, N.V. Durnev, V.V. Kalaev, Analysis of 3D unsteady melt flow and crystallization front geometry during a casting process for silicon solar cells, J. Cryst. Growth 303 (2007) 236–240.
[7] D. Vizman, J. Friedrich, G. Mueller, 3D time-dependent numerical study of the influence of the melt flow on the interface shape in a silicon ingot casting process, J. Cryst. Growth 303 (2007) 231–235.
[8] A. Popescu, D. Vizman, Numerical study of melt convection and interface shape in a pilot furnace for unidirectional solidification of multicrystalline silicon, Cryst. Growth Des. 12 (2011) 320–325.
[9] C. Tanasie, D. Vizman, J. Friedrich, Numerical study of the influence of different types of magnetic fields on the interface shape in directional solidification of multi-crystalline silicon ingots, J. Cryst. Growth 318 (2011) 293–297.
[10] D. Vizman, K. Dadzis, J. Friedrich, Numerical parameter studies of 3D melt flow and interface shape for directional solidification of silicon in a traveling magnetic field, J. Cryst. Growth 381 (2013) 169–178.
[11] P. Li, S. Ren, D. Jiang, J. Li, L. Zhang, Y. Tan, Effect of alternating magnetic field on the removal of metal impurities in silicon ingot by directional solidification, J. Cryst. Growth 437 (2016) 14–19.
[12] P. Rudolph, Travelling magnetic fields applied to bulk crystal growth from the melt: the step from basic research to industrial scale, J. Cryst. Growth 310 (2008) 1298–1306.
[13] P. Rudolph, F.M. Kieβling, U. Rehse, O. Klein, M. Czupalla, N. Dropka, C. Frank-Rotsch, B. Lux, W. Miller, O. Root, Crystal growth from melt in combined heater-magnet modules, J. Korean Cryst. Growth Cryst. Technol. 19 (2009) 215–222.
[14] N. Dropka, T. Ervik, M. Czupalla, F.M. Kiessling, Scale up aspects of directional solidification and Czochralski silicon growth processes in traveling magnetic fields, J. Cryst. Growth 451 (2016) 95–102.
[15] X. Qi, W. Zhao, L. Liu, Y. Yang, G. Zhong, X. Huang, Optimization via simulation of a seeded directional solidification process for quasi-single crystalline silicon ingots by insulation partition design, J. Cryst. Growth 398 (2014) 5–12.
[16] Q. Yu, L. Liu, Z. Li, P. Su, Global simulations of heat transfer in directional solidification of multi-crystalline silicon ingots under a traveling magnetic field, J. Cryst. Growth 401 (2014) 285–290.
[17] X. Qi, Numerical Investigation of Heat and Mass Transport and Grain Evolution in Directional Solidification Process for Silicon Ingots (Ph.D. Thesis), Xi'an Jiaotong University, Xi'an, China, 2017.